Transplanted Mouse Embryonic Stem Cell–Derived Retinal Ganglion Cells Integrate and Form Synapses in a Retinal Ganglion Cell-Depleted Mouse Model

You-Ren Wu,[1,2] Tomoyo Hashiguchi,[1] Junki Sho,[1] Shih-Hwa Chiou,[2] Masayo Takahashi,[1,3] and Michiko Mandai[1]

[1]Laboratory for Retinal Regeneration, RIKEN Center for Biosystems Dynamics Research, Kobe, Japan
[2]Institute of Pharmacology, School of Medicine, National Yang Ming Chiao Tung University, Taipei, Taiwan
[3]Vision Care Cell Therapy, Inc., Kobe, Japan

Correspondence: Michiko Mandai, Laboratory for Retinal Regeneration, RIKEN Center for Biosystems Dynamics Research, 2-2-3 Minatojima-minamimachi, Chuo-ku, Kobe, Hyogo 650-0047, Japan; michiko.mandai@riken.jp.

Received: February 25, 2021
Accepted: October 3, 2021
Published: October 27, 2021

Citation: Wu YR, Hashiguchi T, Sho J, Chiou SH, Takahashi M, Mandai M. Transplanted mouse embryonic stem cell–derived retinal ganglion cells integrate and form synapses in a retinal ganglion cell-depleted mouse model. *Invest Ophthalmol Vis Sci.* 2021;62(13):26. https://doi.org/10.1167/iovs.62.13.26

Purpose. Retinal ganglion cell (RGC) transplantation is a therapeutic approach to replace irreversibly degenerated RGCs in diseases such as glaucoma. However, the application of primary RGCs is limited by the availability of tissues. The goal of this study was to evaluate whether transplanted mouse embryonic stem cell (mESC)-derived RGCs can integrate into the host retina and form cell connectivity with host cells.

Methods. In this study, we prepared small retinal fragments containing RGC as THY1-enhanced green fluorescent protein (EGFP)$^+$ cells from mESCs and placed them near the retinal surface in the air-injected mouse eyes with or without *N*-methyl-D-aspartate (NMDA)-induced RGC depletion. After transplantation, THY1-EGFP$^+$ cell integration was observed in whole-mounts and with immunostaining for synaptic markers.

Results. Transplanted THY1-EGFP$^+$ cells survived for 12 weeks and extended neurites into the inner plexiform layer (IPL) of the host retina. Presumptive synapse formation was identified between grafted RGCs and host bipolar cells. The ratio of transplanted eyes with integration of THY1-EGFP$^+$ neurites in the host IPL was higher in RGC-injured mice compared with healthy controls.

Conclusions. This report shows the potential for therapeutic use of pluripotent cell–derived RGCs by grafting the cells in healthy conditions and with an appropriate technical approach.

Keywords: retinal ganglion cells, transplantation, glaucoma, mouse embryonic stem cells

Central nervous system (CNS) neurons generally lack the capacity to repair and regenerate from neuronal death caused by diseases or injury.[1] Replacing neurons by transplantation is a promising approach for non-treatable diseases. The retina, known as a part of the CNS,[2] consists of diverse retinal cells, including photoreceptors, as the primary apparatus to convert light to electric signals and retinal ganglion cells (RGCs), which convey the neural signal to the brain via a long axon bundled in the optic nerve. Death of RGCs can lead to severe visual loss. Glaucoma is one of the most prevalent eye diseases characterized by progressive degeneration of RGCs and permanent blindness, partly resulting from high intraocular pressure (IOP).[3] For the purposes of slowing disease progression, current treatments control elevated IOP through the use of medication and surgery. However, the loss of RGCs is irreversible, so the development of other therapies is necessary.

In previous studies, several cell-based therapies for glaucoma and optic neuropathies have been reported. For example, bone marrow–derived Lin-ve stem cells,[4] human periodontal ligament–derived stem cells,[5] and mesenchymal stem cells[6] have neuroprotective effects that prevent cell death and promote axonal regeneration in a rodent model of RGC degeneration. In addition to stem cells, neural progenitors and mature RGCs have also been used for transplantation in animal models of degeneration. Embryonic stem cell (ESC)-derived neural progenitors transplanted in *N*-methyl-D-aspartate (NMDA)-injected RGC-depleted mice differentiated into RGC lineage and improved visual acuity.[7] A neural progenitor cell line (C17.2) transplanted in superior colliculus–ablated mice and ON-transected mice expressed the neural marker beta III tubulin, but grafted cells did not express the retinal markers POU4F2 and PAX6.[8] The integration of transplanted adult hippocampal precursor cells with host retina was increased by neuropeptide somatostatin pretreatment.[9] Those studies also observed the increased integration in RGC depleted retinas compared with intact retinas.[8,9] Furthermore, mature primary RGCs that have been transplanted into rat retinas demonstrated light responses.[10] Even when two different sources of cells were combined, co-transplantation of primary RGCs and human-induced pluripotent stem cells (hiPSCs) promoted transplanted RGC survival and neurite outgrowth.[11] However, the application of primary RGCs is limited by the availability of tissues,

Copyright 2021 The Authors

This work is licensed under a Creative Commons Attribution-NonCommercial-NoDerivatives 4.0 International License.

Downloaded from abstracts.iovs.org on 04/20/2024

and less progress has been made in using ESC/iPSC-derived RGCs as the source of cells for cell replacement in RGC-degenerated animal models.

In this study, we aimed to evaluate whether transplanted mouse embryonic stem cell (mESC)-derived RGCs can integrate into the host retina and form cell connectivity with host cells. Based on previous studies,[12,13] the procedure of RGC isolation would cause cell death and lower their viability in long-term cultures, so we differentiated the THY1-EGFP mESC line into retinal organoids (mESC-retinas) and manually excised the THY1-enhanced green fluorescent protein $(EGFP)^+$ cell clumps as a graft. Furthermore, we comparatively observed whether NMDA treatment might increase the evidence of extending neurites of transplanted RGCs into recipient retinas. Our results provide an option for transplantation strategies to enhance RGC integration and the potential to develop cell therapy for RGC degeneration.

Methods

Differentiation of mESCs into RGCs

The procedure to induce early stages of retinal differentiation was based on a previously described protocol with several modifications.[14] Briefly, THY1-EGFP mESCs were maintained in ESC maintenance medium containing Glasgow's Minimum Essential Medium (GMEM) (Thermo Fisher Scientific, Waltham, MA, USA), 10% (v/v) fetal bovine serum (Biological Industries USA, Cromwell, CT, USA), 0.1-mM non-essential amino acids (Thermo Fisher Scientific), 1-mM sodium pyruvate (Sigma-Aldrich, St. Louis, MO, USA), 0.1-mM 2-mercaptoethanol (Wako Chemicals, Richmond, VA, USA), 100-U/mL penicillin–streptomycin (Thermo Fisher Scientific), 1000 U/mL ESGRO Leukemia Inhibitory Factor (Sigma-Aldrich), 3-µM CHIR 99021 (BioVision, Milpitas, CA, USA), and 1-µM PD0325901 (Stemgent, Cambridge, MA, USA) on gelatin-coated dishes and passaged every 3 to 4 days. On day 0 of differentiation, mESCs were enzymatically detached by 0.25% (w/v) trypsin–EDTA treatment, dissociated into small clumps, and cultured in a suspension containing retinal differentiation medium with GMEM, 5% Knockout Serum Replacement (Thermo Fisher Scientific), 0.1-mM non-essential amino acids (Thermo Fisher Scientific), 1-mM sodium pyruvate (Sigma-Aldrich), 0.1-mM 2-mercaptoethanol (Wako Chemicals), and 0.1-mM AGN 193109 (Toronto Research Chemicals, North York, ON, Canada) to induce embryoid body (EB) formation with 5000 cells/100 µL per well in 96-well U-bottom plates (Thermo Fisher Scientific) and 2% Matrigel (Corning Inc., Corning, NY, USA) after a day. On day 7, EBs were transferred into retinal maturation medium 1 (RMM1) containing Dulbecco's Modified Eagle Medium/Nutrient Mixture F-12 (DMEM/F-12) with GlutaMAX (Thermo Fisher Scientific), 1% N-2 supplement (Thermo Fisher Scientific), and 100-U/mL penicillin–streptomycin (Thermo Fisher Scientific). On day 10, the aggregates were switched to retinal maturation medium 2 (RMM2) containing DMEM/F-12 with GlutaMAX, 1% N-2 supplement, 100-U/mL penicillin–streptomycin, 10% (v/v) fetal bovine serum, 0.5-µM all-*trans*-retinoic acid (Sigma-Aldrich), and 0.1-mM L-taurine (Sigma-Aldrich). For adhesion cultures, the neurospheres were transferred on day 14 to poly-D-lysine/laminin-coated dishes with neuron maintenance medium containing Neurobasal Medium (Thermo Fisher Scientific), 2% B-27 supplement (Thermo Fisher Scientific), and 1% GlutaMAX. Thereafter, the medium was changed every 2 to 3 days until day 22.

Animals

All animal experiments were conducted in accordance with local guidelines and the ARVO Statement for the Use of Animals in Ophthalmic and Vision Research. All experimental protocols were approved by the Center for Biosystems Dynamics Research committee. Adult C57BL/6N mice were obtained from the RIKEN BRC animal experiment committee. All mice were housed under a standard 12-hour light/dark cycle.

Graft Preparation and Transplantation of mESC-RGC–Containing Retinal Tissues

For graft preparation, mESC-RGC cell clumps were prepared from differentiated day 14 mESC retinas. THY1-$EGFP^+$ dense area was manually excised from mESC retinas (pieces approximately 0.2 mm by 0.3 to 0.5 mm) as a clump by using 18-gauge and 26-gauge needles (Terumo Corporation, Tokyo, Japan) (see Fig. 2A) and kept in Hanks' Balanced Salt Solution (Thermo Fisher Scientific) on ice. For mESC-RGC transplantation, C57BL/6N mice (6–8 weeks old) were anesthetized by inhalation of 2% to 4% isoflurane. Pupils were dilated with Mydrin-P (0.5% phenylephrine, 0.5% tropicamide; Santen Pharmaceutical, Osaka, Japan). Benoxil (0.4% oxybuprocaine hydrochloride; Santen Pharmaceutical) was used for corneal anesthetization when needed. The eye was gently pressed to allow some vitreous to escape from the eye to lower the intraocular pressure. Then, 5 µL of room air was injected intravitreally, followed by a mESC-RGC clump using glass pipettes as previously described,[15] which allowed for the transplanted tissue to settle at the bottom of the air, staying close to the retinal surface (see Fig. 4A). On the average, a clump contained 26166 ± 3465 cells ($n = 6$ clumps). Transplanted mice were sacrificed between 1 and 3 months after transplantation for whole-mount immunofluorescence staining.

Immunofluorescence Staining

Immunofluorescence staining was performed using the indicated antibodies. For adhesion cultures, mESC retinas were cultured in poly-D-lysine/laminin–coated 35-mm glass-bottom dishes (Matsunami Glass, Osaka, Japan). The cells were fixed in 4% (w/v) paraformaldehyde for 10 minutes at room temperature and washed three times with PBS. A permeabilization step utilizing 3% (v/v) Triton 100-X in PBS was performed prior to staining with antibodies for internal cell markers. Non-specific staining was blocked by incubation in 1% (w/v) bovine serum albumin (Sigma-Aldrich) in PBS overnight at 4°C. The cells were incubated with primary antibodies for 3 to 7 days at 4°C. Following this incubation, cells were washed three times for 10 minutes each with PBS and then incubated with the corresponding secondary antibodies for 2 to 3 days at 4°C. For whole retinal immunostaining, the eyes were fixed for 30 to 60 minutes with 4% (w/v) paraformaldehyde, and the retina was dissected from the eye cup; the rest of the protocol was the same as for adhesion culture cell immunostaining. The primary and secondary antibodies used in this study are presented in Table 2. Three-dimensional images were obtained using a TCS

Investigative Ophthalmology & Visual Science

Downloaded from abstracts.iovs.org on 04/20/2024

SP8 laser scanning confocal microscope (Leica, Wetzlar, Germany).

Reverse-Transcription PCR

Total RNA (1 µg) was purified with Invitrogen TRIzol reagent (Thermo Fisher Scientific), and cDNA was synthesized using SuperScript III First-Strand Synthesis SuperMix (Thermo Fisher Scientific) according to the manufacturer's instructions. PCR was performed using the SapphireAmp Fast PCR Master Mix (Takara Bio, Shiga, Japan). The gene-specific primer sequences are presented in Table 3.

Flow Cytometry

The THY1-EGFP$^+$ part of the mESC retina was first excised using the same procedure as for graft preparation for transplantation on differentiation day 14. The clumps were then dissociated into single-cell suspensions in Accutase (Sigma-Aldrich) for 15 minutes at 37°C. After blocking with 1% serum, the cell suspension was incubated with 7-aminoactinomycin D (BD Biosciences, Franklin Lakes, NJ). All samples were examined with a BD FACSCantoTM II flow cytometer (BD Biosciences), and data were analyzed using FlowJo software. The gating or sorting strategies for all flow cytometry analyses in this study are shown in Supplementary Figure S1.

In Vivo Ocular Imaging

Spectral-domain ocular coherence tomography (SD-OCT) images were obtained for in vivo imaging to monitor retinal degeneration and graft survival using the Envisu R2200 VHR SDOCT (Bioptigen, Inc., Durham, NC, USA). Fluorescein fundus imaging was performed to confirm the presence of graft tissue using a Heidelberg retina angiograph (Heidelberg Engineering, Heidelberg, Germany).

Induction of RGC Death by NMDA in Mouse Eyes

NMDA-induced RGC damage in the mouse eye was conducted as previously described.[16] Briefly, C56BL/6 mice 6 to 8 weeks of age were anesthetized and intravitreally injected with 2 µL of 0.1-mM, 1-mM, 10-mM, 30-mM, and 100-mM NMDA in PBS. An equal volume of PBS was injected as a control. For the remaining RGC counting, 1 week after NMDA injection the animals were sacrificed, and the retinal samples were prepared for analysis.

Quantification of Immunoreactivity of Glial Fibrillary Acidic Protein and Ionized Calcium-Binding Adapter Molecule 1

Mice retinal whole-mounts of healthy control (n = 3 retinas), NMDA treatment (n = 3 retinas), transplantation (n = 3 retinas), and transplantation with NMDA treatment (n = 3 retinas) were photographed using an FV3000 confocal microscope (Olympus, Tokyo, Japan). Image analyses were performed using Fiji software. All of the confocal images of glial fibrillary acidic protein (GFAP) and ionized calcium-binding adapter molecule 1 (IBA1) immunostaining were made with a 40× objective, giving an area of 318 µm (x-axis) × 318 µm (y-axis) per field analyzed. For the quantification of GFAP$^+$ area, a thickness of 10 µm for the x-axis and y-axis was selected for each retinal whole-mount in both the x,z and y,z planes, including all of the retinal layers. For the quantification of IBA1$^+$ area and IBA1$^+$ cells, an area of 318 µm (x-axis) × 318 µm (y-axis) was selected for each retinal whole-mount in the x,y plane, including all of the retinal layers. During quantitation, RGB images were converted to 32-bit grayscale images. The grayscale images were adjusted for brightness and contrast to exclude noise pixels. For the quantification of GFAP$^+$ and IBA1$^+$ areas, images were thresholded to highlight all positive pixels to be measured. IBA1$^+$ cells were quantified by manually counting.

Statistical Analysis

Data are presented as mean ± SEM and analyzed using Excel (Microsoft, Redmond, WA, USA). The statistical analysis was performed using Student's t-test or one-way ANOVA. The difference was considered significant when $P < 0.05$.

Results

Differentiation of mESCs Into RGCs

In order to differentiate THY1-EGFP mESCs into RGCs, we used a stepwise protocol that we described previously to obtain mESC retinas,[14,15] based on different cell culturing conditions and morphogenic factors applied at appropriate times, as outlined in Figure 1A. Briefly, mESCs were induced to form embryoid bodies by culturing them in a suspension culture, followed by the formation of optic cups. The latter were induced to differentiate into RGCs by cultivating the neuronal culture supplement N-2 (Fig. 1A). In order to confirm the identity of the differentiated RGCs, we aimed to detect the expression of the neuron-specific marker and RGC-specific marker. The neurite marker protein β-tubulin isotype III (TUBB3; beta III tubulin), the dendrite marker protein microtubule-associated protein 2 (MAP2), and the RGC marker proteins THY1-EGFP and POU domain, class 4, transcription factor 1 (POU4F1) were detected by immunofluorescence assay (Fig. 1B). Other retinal markers confirmed that the organoids were of retinal lineage, such as neural retinal progenitor marker mRNAs *Rax*, *Pax6*, and *Vsx2*; photoreceptor marker mRNA *Crx*; horizontal cell marker mRNA *Calb1*; bipolar cell marker mRNA *Prkca*; and retinal pigment epithelium (RPE) marker mRNA *Mitf*. The markers for retinal ganglion cell *Atoh7*, *Pou4f2*, and *Isl1* were also detected by reverse transcription (RT)-PCR, thus confirming that the applied protocol generated differentiated retinal cells (Fig. 1C). The expression of RGC markers was observed from differentiated day 7 and the highest expression on differentiated day 14, the transplant day in the next step of the experiment.

Preparation of Graft Tissue and THY1-EGFP$^+$ Cell Content

As a proof-of-concept study, for proper targeting of graft cells on the host retina with substantial graft cell survival, we decided to use THY1-EGFP$^+$ tissue by manually excising them from mESC retinas on differentiated day 14 (Figs. 2A, 2B). Using flow cytometry, we found that THY1-EGFP expression increased from day 7 to day 14 (Fig. 2C). We estimated the percentage of THY1-EGFP$^+$ cells to be 0.78% ± 0.21% in differentiated day 7 embryoid bodies,

Investigative Ophthalmology & Visual Science

Downloaded from abstracts.iovs.org on 04/20/2024

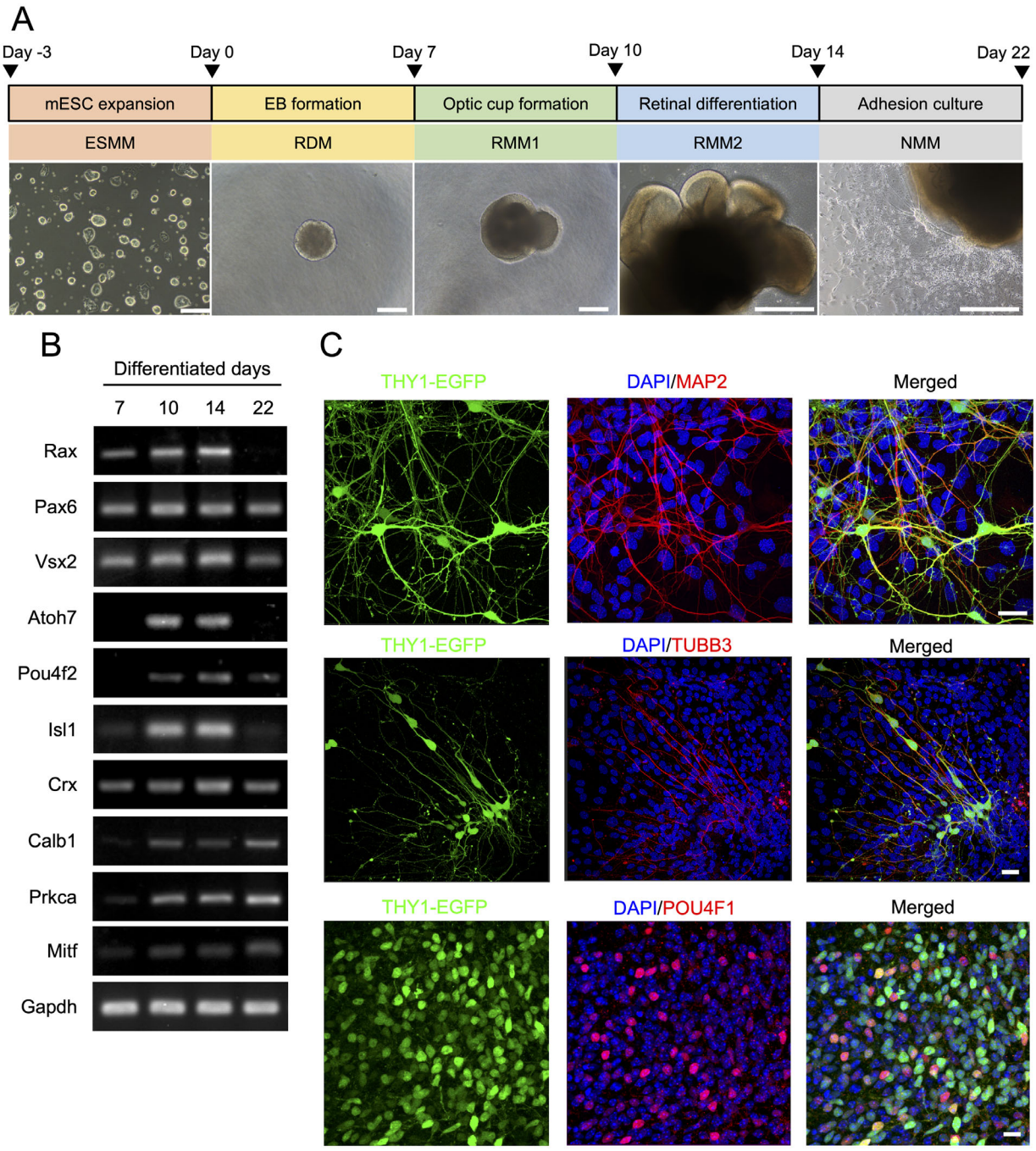

Figure 1. Differentiation of THY1-EGFP mESCs into mESC retinas with RGC marker expression. (**A**) Schematic diagram of the protocol for mESC retina differentiation from THY1-EGFP mESCs. Optical micrographs of each differentiation stage from DD1 to DD22 are also shown. *Scale bars*: 200 µm. (**B**) RT-PCR analysis of mRNA expression of neural retinal progenitor markers Rx, Pax6, and Chx10; retinal ganglion cell markers Atoh7, Pou4f2, and Isl1; photoreceptor marker Crx; horizontal cell marker Calb1; bipolar cell marker Prkca; and retinal pigment epithelium marker Mitf at DD7, DD10, DD14, and DD22. Amplification of GAPDH mRNA was used as an internal control. NTC, no template control. (**C**) Immunofluorescent staining of DD22 mESC retinas in adhesion culture showing expression of RGC markers THY1-EGFP (cell surface) and POU4F1 (nuclear) neurite markers MAP2 and TUBB3. Nuclei were stained with DAPI. *Scale bars*: 30 µm.

3.57% ± 0.29% in differentiated day 14 mESC retinas, and 23.47% ± 1.60% in differentiated day 14 graft tissue after manually excised isolation (Fig. 2D). Thus, we characterized the spatiotemporal pattern of RGCs in mESC retinas and verified the population of THY1-EGFP$^+$ cells in donor cells.

Induction of RGC Depletion by NMDA Injection in Mouse Retina

To optimize NMDA concentrations in this excitotoxicity model, we intravitreally injected 0.1-mM, 1-mM, 10-mM, 30-mM, and 100-mM NMDA and PBS as control (Fig. 3A).

Investigative Ophthalmology & Visual Science

Downloaded from abstracts.iovs.org on 04/20/2024

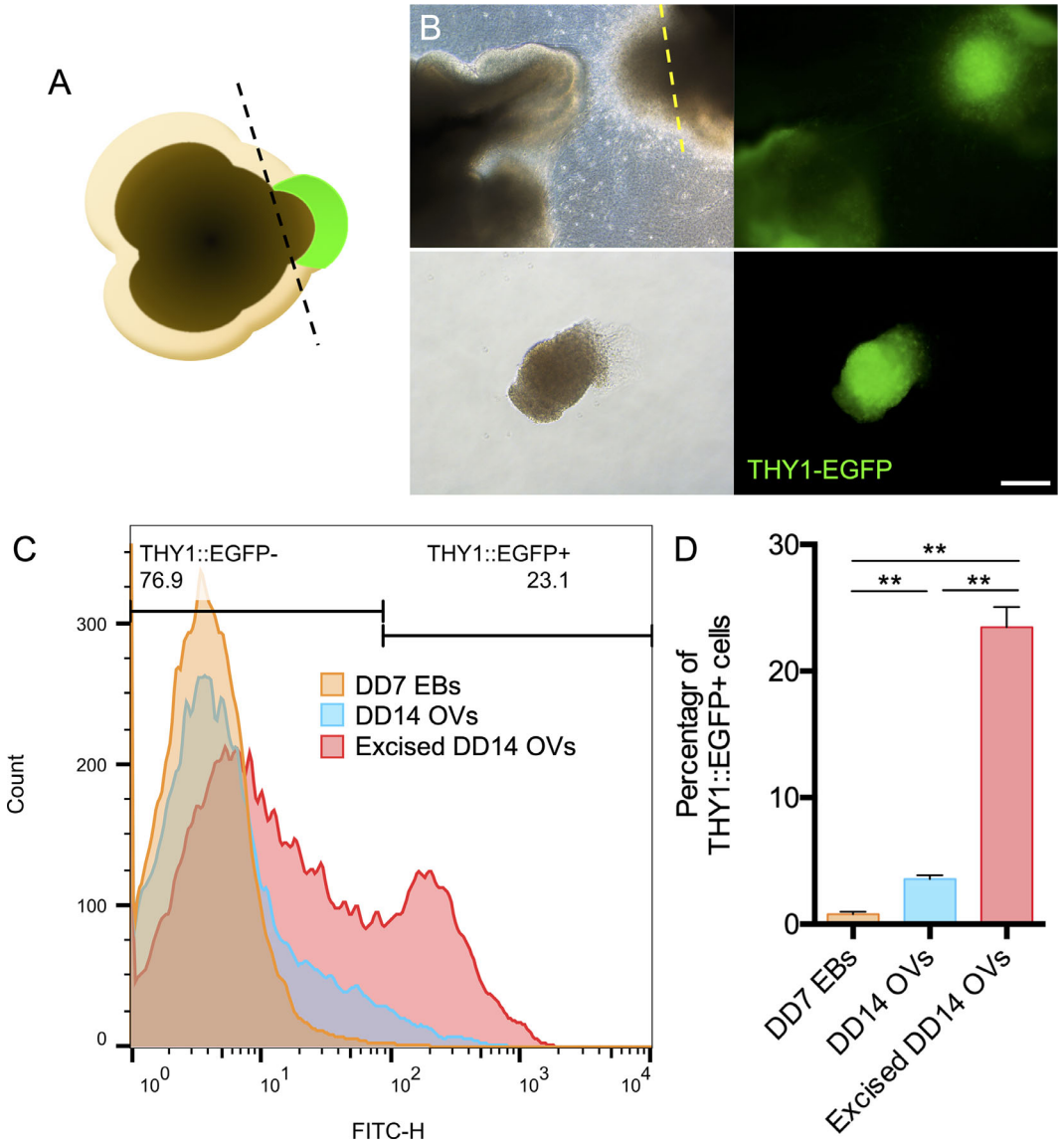

Figure 2. Analysis of THY1-EGFP$^+$ cell population in mESC-RGC graft tissues. (**A**) Schematic of manual isolation of THY1-EGFP$^+$ tissue from mESC retina. (**B**) THY1-EGFP expression in the DD14 mESC retinas differentiated from THY1-EGFP mESCs. Bright-field (*left panels*) and fluorescence (*right panels*) images of DD14 mESC retinas before (*upper panels*) and after (*lower panels*) manual isolation indicating that the THY1-EGFP$^+$ component (*yellow line*) was excised for transplantation. *Scale bar*: 100 µm. (**C**) Flow cytometry analysis showing THY1-EGFP$^+$ rates for the DD7 embryoid body (*orange*), DD14 mESC retinas (*blue*), and excised DD14 mESC retinas (*red*). (**D**) Percentages of THY1-EGFP$^+$ cells in the DD7 embryoid body (*orange*), DD14 mESC retinas (*blue*), and excised DD14 mESC retinas (*red*) determined by flow cytometry analysis (DD7 EBs, 0.78% ± 0.21%; DD14 optic vesicles, 3.75% ± 0.29%; excised DD14 optic vesicles, 23.47% ± 1.60%; $n = 3$ independent experiments per group). Data are represented as the mean ± SEM. Asterisks indicate statistically significant differences (**$P < 0.01$, ANOVA test).

One week after injection, whole-mount retinas were stained with the RGC marker RNA-binding protein with multiple splicing (RBPMS) for counting RGC numbers. Square areas (400 µm × 400 µm), which were 600 µm (central), 1200 µm (middle), and 1800 µm (peripheral) away from the optic disc in each of the four retinal quadrants, were defined as the measured area (Fig. 3C). In the central area of the retina, 30-mM and 100-mM NMDA injections induced a significant loss of RGCs as compared with PBS injection (Fig. 3B). In the quantitative data, the trend was observed that the cell density of RGCs in the central region of retina was the highest and in the peripheral region of the retina was the lowest (Fig. 3D). Furthermore, the average survival ratios of RGCs in retinas injected with PBS (99.95% survival), 0.1-mM NMDA (99.81% survival), and 1-mM NMDA (98.46% survival) were similar to untreated retinas, and dose-dependent RGC loss was observed in retinas injected with from 10-mM (58.10% survival) to 100-mM (22.41% survival) NMDA. Next, we used OCT to monitor the degree of retinal degeneration based on the thickness of the ganglion cell complex, including the retinal nerve fiber layer (RNFL), ganglion cell layer, and inner plexiform layer (IPL). OCT non-invasively acquires cross-sectional images of the retina so that the morphology of the retina can be monitored in vivo. The OCT images showed that the thickness of the ganglion cell complex was significantly reduced a week after the 30-mM and

Investigative Ophthalmology & Visual Science

Downloaded from abstracts.iovs.org on 04/20/2024

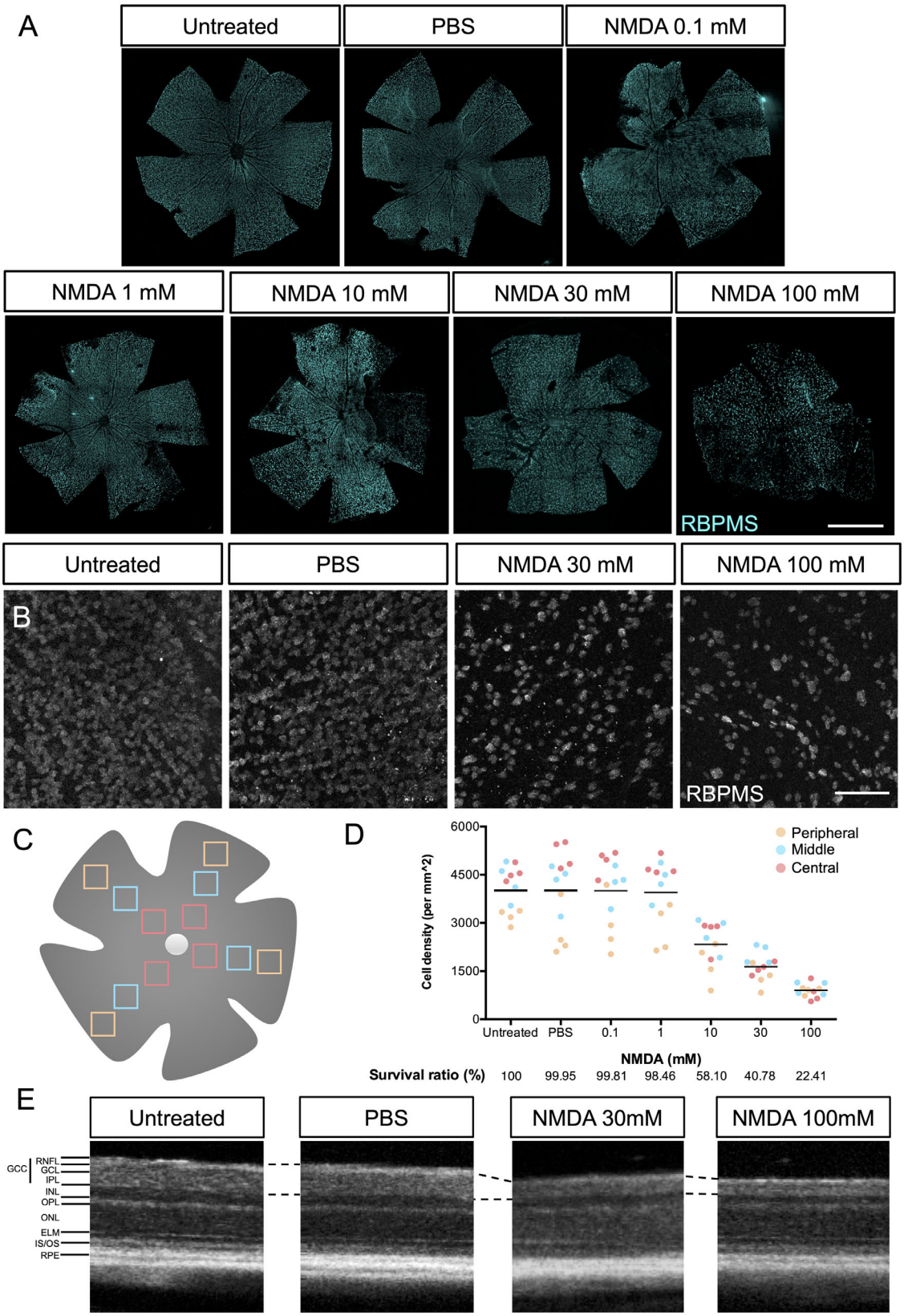

Figure 3. RGC loss after NMDA-induced neurotoxicity in mice. (**A**) RBPMS-stained RGCs of whole-mount mice retinas without injection (untreated) and 1 week after intravitreal injection of 2 µL of PBS, 0.1-mM NMDA, 1-mM NMDA, 10-mM NMDA, 30-mM MMDA, and 100-mM NMDA. *Scale bar*: 1.5 mm. (**B**) Representative images of the central square (400 × 400 µm) of RBPMS-stained RGCs of whole-mount mice retinas at 1 week after intravitreal injection of 2 µL of PBS and 100-mM NMDA. (**C**) Schematic of counted areas in the whole-mount retina squares of 400 × 400 µm were counted at 600 µm (central; *red squares*), 1200 µm (middle; *blue squares*), and 1800 µm (peripheral; *orange*

Investigative Ophthalmology & Visual Science

Downloaded from abstracts.iovs.org on 04/20/2024

squares) from the optic disc in each of the four quadrants of the retina. *Scale bar*: 100 µm. (**D**) The cell numbers of RBPMS$^+$ RGCs in a 1-mm^2 region. The average cell density (*black line*) was calculated as an average composite of 12 images involved in the central (*red*), middle (*blue*), and peripheral (*orange*) areas of whole-mount mice retina. The survival ratio of RGCs was normalized to that of the untreated group. (**E**) OCT cross-sectional images of retinas without injection (untreated; *left*) and 1 week after intravitreal injection of 2 µL of PBS (*center*) and 100-mM NMDA (*right*). INL, inner nuclear layer; OPL, outer plexiform layer; ONL, outer nuclear layer; ELM, external limiting membrane; IS/OS, inner and outer segment junctions, respectively, of the photoreceptor cell.

100-mM NMDA injections compared with the untreated or PBS-injected retinas (Fig. 3E). However, considering that severe cell death and unorganized structure of the retina were observed in mice injected with 100-mM NMDA, we decided to use 30-mM NMDA to induce the RGC-degenerated model in the following experiments.

Survival and Neurite Extension into the Host IPL of Transplanted RGCs

Previous RGC transplantation studies have indicated that most of the transplanted cells were not attached to the host retina but remained in the vitreous cavity, an environment with low neurotrophic survival signals.[11] Therefore, in order to improve the attachment of graft cells to the host retina, we mimicked the fluid–gas exchange in theory and aspirated some vitreous fluid followed by the intravitreal injection of air and THY1-EGFP$^+$ tissue into the air space so that the graft tissue would have a better chance of settling on the host retinal surface (Fig. 4A). Four weeks after transplantation, immunostaining of whole-mount retina consistently showed survival and neurite outgrowth of THY1-EGFP$^+$ cell clumps in the host retina (Fig. 4B). However, EGFP$^+$ neurites were observed near the host optic nerve head (ONH), but we did not confirm the evident entry of graft neurites into the host optic nerve. In addition, fluorescent fundus imaging and OCT imaging also showed grafted cells in vivo 4 weeks after transplantation (Figs. 4C, 4D). Alexa Fluor 546 phalloidin-labeled F-actin accumulated at the leading edge of THY1-EGFP$^+$ neurites a week after transplantation, a relatively early stage of post-transplantation (Fig. 4E). EGFP positivity did not change significantly 12 weeks after transplantation, and THY1-EGFP$^+$ neurites were observed in the host IPL in the sectional views of whole-mount retinas (Fig. 4F). Because both NMDA treatment and transplantation procedures can evoke inflammatory responses that may affect graft integration, we examined the changes of Müller cells and microglia by immunostaining of GFAP and IBA1 in the retinas at 1 week after NMDA treatment and/or transplantation (Supplementary Fig. S2). NMDA treatment, transplantation, and transplantation with NMDA treatment all activated and increased the positivity of Müller cells and microglia by intensity and number, respectively, but there was no significant difference among these three conditions. Additionally, we studied the expression of some inflammatory/protective cytokines—ciliary neurotrophic factor (CNTF), fibroblast growth factor 2 (FGF2), and IL-1β—together with the macrophage/microglia markers CD45 and CD11b (Supplementary Fig. S3). The expression of CNTF, FGF2, and IL-1β increased in the ganglion cell layer 1 week after NMDA treatment but was not evident after transplantation. The morphology of positivity of CD11b and CD45 suggested the presence of resting or mildly activated microglia in IPL similarly in all the NMDA-treated and transplanted retinas, but not many infiltrating cells in the retina from outside the eye. The results demonstrated that NMDA treatment might trigger regenerative responses by increased expression of cytokines that potentiate THY1-EGFP$^+$ cells to integrate into the host IPL with neurite extension.

Presumptive Synapse Formation Between Host Bipolar Cells and Transplanted RGCs

The presumptive synapse formation between donor RGCs and the host retina should be identified as a THY1-EGFP$^+$ dendrite terminal co-localized with the postsynaptic marker DLG4, which contacts the ON bipolar cell marker secretagogin (SCGN) in the host retina (Fig. 5A). Furthermore, to confirm whether SCGN-stained bipolar cells were host cells, we tracked the position of cell bodies through SCGN-stained neurites. The sectional view of the whole-mount retina showed that THY1-EGFP$^+$ neurites co-localized with the postsynaptic marker DLG4 and contacted the axon terminal of bipolar cells whose cell body was in the host INL (Fig. 5B). In addition, synaptic puncta were identified as THY1-EGFP$^+$ neurite terminals co-localized with the postsynaptic marker DLG4 and paired with the ribbon-synaptic marker CTBP2 (Fig. 5C). Overall, these results confirmed that graft RGCs were capable of forming connections with the host retina.

Higher Ratio of Neurite Integration Into the IPL of RGC-Degenerated Retinas

We then compared the efficiency of graft RGC integration and presumptive synapse formation between the normal retinas and NMDA-injected retinas as hosts (Table 1). In successful transplantation, GFP-positive donor RGCs were observed on or in the retinas instead of floating in the vitreous space (success ratio of 11/17 in control eyes and 12/17 in NMDA-injected eyes). The ratio of host retinas with some donor RGCs integrating in the IPL was higher in the retinas with NMDA injection (8/12 eyes, 66.67%) than without NMDA injection (3/11 eyes, 27.27%). In most eyes with donor RGC integration, presumptive synapse formation between graft RGCs and host bipolar cells was identified in both groups. This may indicate that the integration of transplanted cells was the rate-limiting step of successful transplantation. On the other hand, these data suggest a higher potential for RGC integration in NMDA-damaged, RGC-depleted mice compared with healthy controls.

Discussion

Although purification of RGCs is desirable for transplantation, purification of RGCs often leads to cell damage and poor survival after transplantation. In order to test the proof of concept of healthy RGC transplantation for their ability to survive and integrate, we utilized RGC-rich retinal tissue fragments differentiated from mESCs. For this purpose, we differentiated THY1-EGFP mESCs into mESC retinas and manually excised THY1-EGFP$^+$ cell containing fragments

Investigative Ophthalmology & Visual Science

Downloaded from abstracts.iovs.org on 04/20/2024

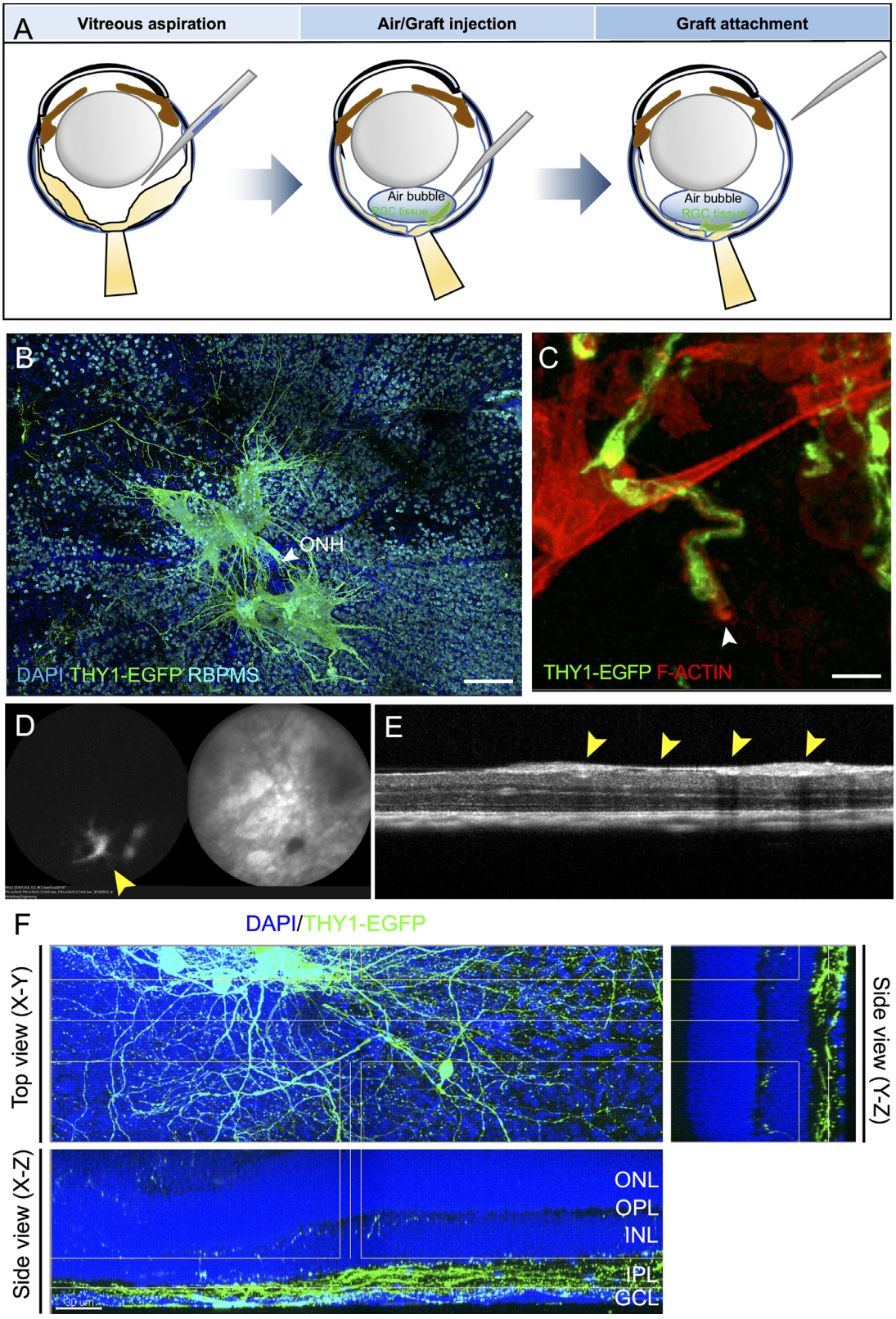

Figure 4. Neurite extension and integration of THY1-EGFP$^+$ cells after transplantation in the host retina. (**A**) Schematic of the procedure for THY1-EGFP$^+$ cell clump transplantation. (**B**) Morphology of THY1-EGFP$^+$ cells at 4 weeks after transplantation in whole-mount mouse retinas with RBPMS immunostaining. *Scale bar*: 150 µm. (**C**) Growth cone (*white arrow*) of THY1-EGFP$^+$ neurites stained with phalloidin to localize filamentous actin (F-actin; *red*) at 1 week after transplantation. *Scale bar*: 5 µm. (**D**, **E**) In vivo imaging of THY1-EGFP mESC-derived retinal cell clumps (*yellow arrows*) at 4 weeks after transplantation: autofluorescence (*left*) and infrared reflectance (*right*) (**D**), and OCT imaging (**E**). (**F**) In the whole-mount mouse retina, THY1-EGFP$^+$ neurites extended and integrated into the host IPL at 12 weeks after transplantation. *Scale bar*: 30 µm.

Investigative Ophthalmology & Visual Science

Downloaded from abstracts.iovs.org on 04/20/2024

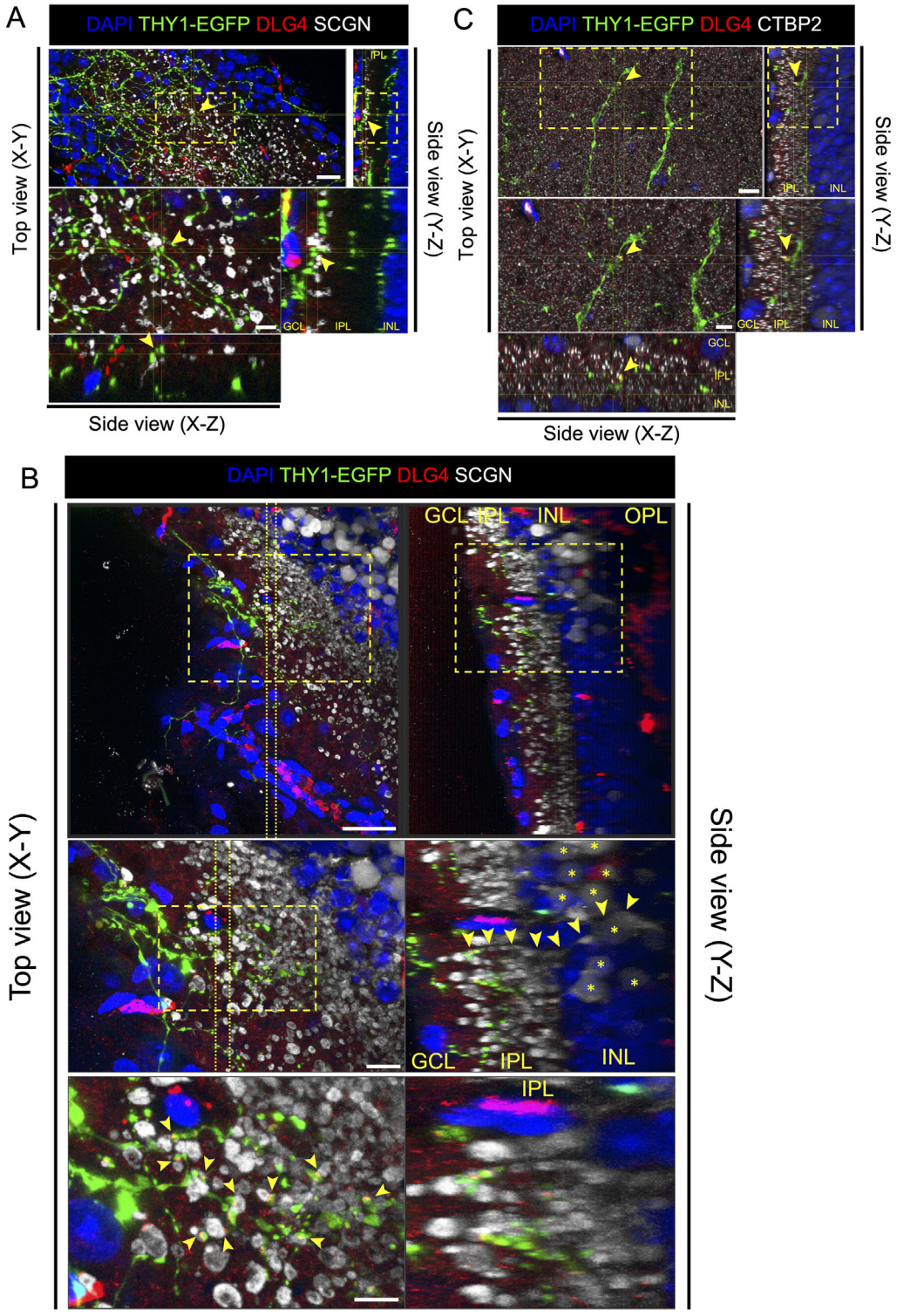

Figure 5. Presumptive synapse formation between transplanted THY1-EGFP$^+$ cells and host bipolar cells after transplantation. (**A**) Four weeks after transplantation in the control eye, three-dimensional confocal images of transplanted area stained with postsynaptic marker DLG4 (*red*) and cone bipolar cell marker SCGN (*white*). DLG4 was co-localized at the contact site (*yellow arrows*) of THY1-EGFP$^+$ cells (*green*) and host bipolar cells. *Scale bars*: 20 µm (*upper panel*) and 6 µm (*lower panel*). (B) Four weeks after transplantation in the NMDA-injected eye, three-dimensional confocal images of transplanted area stained with postsynaptic marker DLG4 (*red*) and cone bipolar cell marker SCGN (*white*). DLG4 was co-localized at the contact site of THY1-EGFP$^+$ cells (*green*) and host bipolar cells (host bipolar cell bodies marked by *yellow asterisks*). A bipolar cell axon (*yellow arrows*) can be traced back from the IPL into the INL of the host retina. *Scale bars*: 30 µm (*upper panel*), 10 µm (*middle panel*), and 6 µm (*lower panel*). (C) Four weeks after transplantation in NMDA-injected eye, three-dimensional confocal images of transplanted area stained with postsynaptic marker DLG4 (*red*) and presynaptic marker CTBP2 (*cyan*). DLG4 was co-localized at the contact site (*yellow arrows*) of THY1-EGFP$^+$ cells (*green*) and CTBP2. *Scale bars*: 20 µm (*upper panel*) and 5 µm (*lower panel*).

Investigative Ophthalmology & Visual Science

Downloaded from abstracts.iovs.org on 04/20/2024

Table 1. Successful Rate of Transplantation in Mice With and Without NMDA Injection

Model	Transplanted Samples With THY1-EGFP$^+$ Cells/Total Transplantations, *n* (%)	Transplanted Samples With THY1-EGFP$^+$ Cells in IPL/Transplanted Samples With THY1-EGFP$^+$ Cells, *n* (%)	Transplanted Samples With Synapse Formation/Transplanted Samples With THY1-EGFP$^+$ Cells in IPL, *n* (%)
Control	11/17 (64.71)	3/11 (27.27)	2/2 (100)
NMDA	12/17 (70.59)	8/12 (66.67)	3/4 (75)

Table 2. Primary and Secondary Antibodies and Their Working Dilutions

Primary Antibodies

Target	Antibody	Species	Dilution	Manufacturer
ATOH7	Anti-ATH5	Rabbit	1:500	MilliporeSigma
MAP2	Anti-MAP2	Mouse	1:500	Sigma-Aldrich
TUBB3	Anti-TUJ1	Mouse	1:500	MilliporeSigma
POU4F2	Anti-BRN3	Goat	1:500	Santa Cruz Biotechnology
RBPMS	Anti-RBPMS	Guinea pig	1:500	MilliporeSigma
DLG4	Anti-PSD95	Mouse	1:500	BioLegend
SCGN	Anti-Segretagogin	Sheep	1:500	BioVendor
CTBP2	Anti-CtBP2	Mouse	1:500	BD Biosciences
GFAP	Anti-GFAP	Mouse	1:500	Cell Signaling Technology
IBA1	Anti-IBA1	Rabbit	1:500	Wako Chemicals
CNTF	Anti-CNTF	Mouse	1:500	MilliporeSigma
FGF2	Anti-FGF-2	Mouse	1:500	MilliporeSigma
IL1B	Anti-IL-1β	Mouse	1:500	Cell Signaling
ITGAM	Anti-CD11b	Rat	1:500	Thermo Fisher Scientific
PTPRC	Anti-CD45	Rat	1:500	BD Biosciences

Secondary Antibodies

Antibody	Dilution	Manufacturer
Donkey anti-Rabbit IgG (H+L) Highly Cross-Adsorbed Secondary Antibody, Alexa Fluor 546	1:1000	Thermo Fisher Scientific
Donkey anti-Mouse IgG (H+L) Highly Cross-Adsorbed Secondary Antibody, Alexa Fluor 647	1:1000	Thermo Fisher Scientific
Donkey anti-Mouse IgG (H+L) Highly Cross-Adsorbed Secondary Antibody, Alexa Fluor 546	1:1000	Thermo Fisher Scientific
Donkey anti-Goat IgG (H+L) Cross-Adsorbed Secondary Antibody, Alexa Fluor 54	1:1000	Thermo Fisher Scientific
Goat anti-Guinea Pig IgG (H+L) Highly Cross-Adsorbed Secondary Antibody, Alexa Fluor 633	1:1000	Thermo Fisher Scientific
Donkey anti-Sheep IgG (H+L) Cross-Adsorbed Secondary Antibody, Alexa Fluor 647	1:1000	Thermo Fisher Scientific
Goat anti-Mouse IgG2a Cross-Adsorbed Secondary Antibody, Alexa Fluor 546	1:1000	Thermo Fisher Scientific
Goat anti-Mouse IgG1 Cross-Adsorbed Secondary Antibody, Alexa Fluor 647	1:1000	Thermo Fisher Scientific

for transplantation into RGC-degenerated mice and healthy controls. Furthermore, our data suggest that mESC-derived RGCs were capable of surviving for at least 3 months, extending neurites, integrating into the IPL of host retinas, and forming synapses with host bipolar cells after transplantation.

Our flow cytometry data indicate that the population of RGCs in mESC retinas (3%–4%) (Fig. 2D) was higher than in the adult mouse retina (<1%)[17] but similar to the other differentiated protocol (<5%).[18] Although the purity of graft cells is often prioritized, neural cells can be damaged after the purification procedure is stripped off from other supportive cells, including glial cells. For the two-step immunopanning method, the survival rate of RGCs was about 50% at 3 days after purification in culture but decreased to about 25% by day 30.[12] For the two-step immunopanning–magnetic method, most RGCs died 9 days after purification in culture.[13] We used manually excised retinal tissues containing 23% THY1-EGFP$^+$ cells to primarily test the potency of mESC-derived RGCs and confirmed their reasonable potency for cell-based therapies, although a higher purity of RGC is indeed desirable for clinical application. Because the other EGFP$^-$ cells in the graft were indistinguishable from host mice retinal cells, we could not trace how these cells affected the host retina any further in the present study. Still, there was no tumor formation and evident destruction of the host retinal structure.

Dose-dependent RGC loss after NMDA injection provided a reproducible animal model to study RGC diseases, including glaucoma.[19] In the present study, a substantial number of graft cells attached to the host retina, and a variable number of cells were observed floating in the vitreous from

Investigative Ophthalmology & Visual Science

Downloaded from abstracts.iovs.org on 04/20/2024

Table 3. RT-PCR Primers

Primer Name	Sequence
Rax_forward	GACTCGAAGCTGTCGGAGGAGGAAC
Rax_reverse	CTTTCCGATGGCCTGGATGTGCTCTTTG
Pax6_forward	ACTAAGGATGTTGAACGGGCAGAC
Pax6_reverse	GCTGTGGGATTGGCTGGTGGTAGA
Vsx2_forward	TTCTACACACAGCCCACCTT
Vsx2_reverse	CGACTTTTTGTGCATCCCCA
Atoh7_forward	ACAAGAAGCTGTCCAAGTAC
Atoh7_reverse	AATGGCCCCGAGGCTTAGCTG
Pou4f2_forward	TTGTCTTCCAACCCCACCGA
Pou4f2_reverse	GGTTCATGGTGGCCATGTGT
Isl1_forward	CGTCTGATTTCCCTGTGTGTTGGTTGC
Isl1_reverse	CGTTCTTGCTGAAGCCTATGCTGCACTTG
Crx_forward	GGCATAAGGGGCTGAGGTGAGAGAG
Crx_reverse	CTTGGCTCTGAGTGGCCCCAATGTG
Calb1_forward	CTGCAGTCATCTCTGATCACAGCCTCACAG
Calb1_reverse	CGGTACAGCTTCCCTCCATCCGACAAG
Prkca_forward	CTGCAGCCACTGCACCGACTTCATC
Prkca_reverse	GAGTCGTCCGATCCCAGTCCCAGATTTC
Mitf_forward	CCCGTCTCTGGAAACTTGATCG
Mitf_reverse	CTGTACTCTGAGCAGGTG
Gapdh_forward	GCTCATGACCACAGTCCATGCCATCAC
Gapdh_reverse	CATCGAAGGTGGAAGAGTGGGAGTTGCTG

sample to sample. In an attempt to quantify the efficiency of mESC-RGC transplantation in the retinas with and without RGC depletion, we adopted an approach that is both qualitative and quantitative by counting the eyes with or without a presentation of neurite extension into the IPL and presumptive synapse formation by graft cells (Table 1). Interestingly, our results showed a greater number of eyes with integration of transplanted RGC into the host IPL in the NMDA-injected retinas compared with uninjured controls (Table 1). In a previous study, the barriers to RGC integration of transplanted cells have been reported, such as the inner limiting membrane (ILM)[20] and glial cell reactivity.[21] NMDA-induced degeneration may have affected the barrier features of the ILM or RGC layer. In addition, another possibility for favorable graft RGC integration was the activation of endogenous neuroprotective responses after retinal injury. Several neurotrophic factors are expressed after NMDA intravitreal injection to promote neuroregeneration, such as brain-derived neurotrophic factor in the retina[22,23] and in the superior colliculus,[24] and CNTF in the retina.[25]

Generally, the low efficiency of RGC transplantation would be due to the fact that most of the transplanted cells often remain in the vitreous cavity, which is an environment with low neurotrophic survival signals.[11] Based on this consideration, we injected the graft tissue at the bottom of the injected air bubble, which theoretically mimicked the routine fluid–air exchange after vitrectomy in clinical practice. It kept the graft close to the retinal surface, increasing the chances of it attaching to the retina instead of floating around in the midst of the vitreous cavity. Additionally, the intravitreal injection combined with vitreous aspiration has been reported to improve the transduction efficiency of adeno-associated virus (AAV)2/8, which may be caused by the formation of holes in the ILM, allowing AAV particles to diffuse into the retina.[26] The procedure of fluid–gas exchange followed by graft placement on the retinal surface, with or without ILM peeling, should be worth testing in a larger animal models in view of clinical applications of RGC transplantation in the future.

In the present study, there was no evidence of THY1-EGFP$^+$ axons extending into the host optic nerves, indicating that we still lack some signal for visual pathway reconstruction. Multiple molecular mechanisms participate in RGC axon guidance from the eye to the brain. For example, chondroitin sulfate proteoglycans and Slit2, expressed in a low central, high peripheral gradient, drive axonal extension from the peripheral retina to the optic disk by inhibitory signaling.[27–29] On the other hand, Sonic hedgehog is expressed in an opposite gradient, centrally promoting the growth of RGC axons.[30] Another key molecule required for RGC axon growth into the optic nerve is Netrin-1 and its receptor, deleted in colorectal cancer (DCC), on growth cones of the RGC axon.[31] Netrin-1, expressed by optic disc glial cells, initially attracts RGC axons, but after that it becomes repulsive and drives the axon out of the optic disc by changing cAMP levels in the growth cone of the RGC.[32] It has been reported the expression of Netrin-1 and DCC are downregulated in the injured retina,[33,34] so lack of proper signal of axon guidance may explain why we did not observe an extensive elaboration of filopodia in the growth cone of the graft (Fig. 4C).[35] Transplanting RGCs with the gradient Netrin-1–coated biomaterials would be a potential strategy to guide the RGC axon to the host ONH.[36] On the other hand, although Netrin-1 and its receptor DCC have been identified in cultured human ESC-RGCs,[37] further investigation of the axon guidance receptor and its downstream pathway in transplanted mESC-RGC would be required to promote the technology for RGC transplantation therapy in clinical applications.

Neuroinflammation is known to play an important role in the CNS injury, including NMDA-induced retinal excitotoxicity.[38] Previous studies have shown that NMDA injection activates Müller cells[39] and microglia[40] and induces macrophages infiltration[41] in the rodent retina. In the present study, activation of microglia seemed moderate, and there was no evident infiltration of macrophages inside the retina. Still, NMDA treatment enhanced the expression of some cytokines (Supplementary Fig. S3), including CNTF, which may promote the regenerative potency of resident RGCs.[42–44] The role of these cytokines must be further investigated to understand how they affect the integration and neurite extension of grafted RGCs. Overall, the inflammatory process may affect the outcomes of the transplantation, the safety of clinical applications,[45] the differentiation of transplanted cells,[46,47] and the health of intrinsic cells such as photoreceptors.[48,49] Also, the transplantation itself could also cause an immune response due to allogeneic rejection.[50] In this study, NMDA treatment, transplantation, and transplantation with NMDA treatment similarly activated Müller cells and microglia, but there was no significant difference among these three conditions (Supplementary Fig. S2). The use of antiinflammatory drugs such as glucocorticoids with ESC/iPSC-derived RGCs transplantation must be further evaluated for better RGC integration in the future.

In conclusion, mESCs were differentiated into mESC retinas, and some of THY1-EGFP$^+$ cells were excised as grafts. After transplantation into the mouse model, graft RGCs survived for 12 weeks, extended neurites into the host IPL, and some eventually connected with host bipolar cells. Interestingly, we found a greater number of eyes with successful transplantation, as judged by graft integration and presump-

Investigative Ophthalmology & Visual Science

Downloaded from abstracts.iovs.org on 04/20/2024

tive synapse formation, in the RGC-injured model. This report indicates the theoretical potential of using pluripotent cell-derived RGCs by grafting healthy cells and using an appropriate technical approach.

Acknowledgments

The authors thank Akishi Onishi for supplying THY1-EGFP mESCs and Hung-Ya Tu for constructive discussion.

Supported by a grant from the Ministry of Science and Technology, Taiwan (MOST 107-2923-B-010-002-MY2).

Disclosure: **Y.-R. Wu**, None; **T. Hashiguchi**, None; **J. Sho**, None; **S.-H. Chiou**, None; **M. Takahashi**, None; **M. Mandai**, None

References

1. Bjorklund A, Lindvall O. Cell replacement therapies for central nervous system disorders. *Nat Neurosci*. 2000;3:537–544.
2. London A, Benhar I, Schwartz M. The retina as a window to the brain-from eye research to CNS disorders. *Nat Rev Neurol*. 2013;9:44–53.
3. Quigley HA. Neuronal death in glaucoma. *Prog Retin Eye Res*. 1999;18:39–57.
4. Jindal N, Banik A, Prabhakar S, Vaiphie K, Anand A. Alteration of neurotrophic factors after transplantation of bone marrow derived Lin-ve stem cell in NMDA-induced mouse model of retinal degeneration. *J Cell Biochem*. 2017;118:1699–1711.
5. Cen LP, Ng TK, Liang JJ, et al. Human periodontal ligament-derived stem cells promote retinal ganglion cell survival and axon regeneration after optic nerve injury. *Stem Cells*. 2018;36:844–855.
6. Mesentier-Louro LA, Teixeira-Pinheiro LC, Gubert F, et al. Long-term neuronal survival, regeneration, and transient target reconnection after optic nerve crush and mesenchymal stem cell transplantation. *Stem Cell Res Ther*. 2019;10:121.
7. Divya MS, Rasheed VA, Schmidt T, Lalitha S, Hattar S, James J. Intraocular injection of ES cell-derived neural progenitors improve visual function in retinal ganglion cell-depleted mouse models. *Front Cell Neurosci*. 2017;1:295.
8. Mellough CB, Cui Q, Spalding KL, et al. Fate of multipotent neural precursor cells transplanted into mouse retina selectively depleted of retinal ganglion cells. *Exp Neurol*. 2004;186:6–19.
9. Mellough CB, Cui Q, Harvey AR. Treatment of adult neural progenitor cells prior to transplantation affects graft survival and integration in a neonatal and adult rat model of selective retinal ganglion cell depletion. *Restor Neurol Neurosci*. 2007;25:177–190.
10. Venugopalan P, Wang Y, Nguyen T, Huang A, Muller KJ, Goldberg JL. Transplanted neurons integrate into adult retinas and respond to light. *Nat Commun*. 2016;7:10472.
11. Wu S, Chang KC, Nahmou M, Goldberg JL. Induced pluripotent stem cells promote retinal ganglion cell survival after transplant. *Invest Ophthalmol Vis Sci*. 2018;59:1571–1576.
12. Zhang XM, Li Liu DT, Chiang SW, et al. Immunopanning purification and long-term culture of human retinal ganglion cells. *Mol Vis*. 2010;16:2867–2872.
13. Gao F, Li T, Hu J, Zhou X, Wu J, Wu Q. Comparative analysis of three purification protocols for retinal ganglion cells from rat. *Mol Vis*. 2016;22:387–400.
14. Kobayashi W, Onishi A, Tu HY, et al. Culture systems of dissociated mouse and human pluripotent stem cell-derived retinal ganglion cells purified by two-step immunopanning. *Invest Ophthalmol Vis Sci*. 2018;59:776–787.
15. Assawachananont J, Mandai M, Okamoto S, et al. Transplantation of embryonic and induced pluripotent stem cell-derived 3D retinal sheets into retinal degenerative mice. *Stem Cell Reports*. 2014;2:662–674.
16. Seitz R, Tamm ER. *N*-methyl-D-aspartate (NMDA)-mediated excitotoxic damage: a mouse model of acute retinal ganglion cell damage. *Methods Mol Biol*. 2013;935:99–109.
17. Jeon CJ, Strettoi E, Masland RH. The major cell populations of the mouse retina. *J Neurosci*. 1998;18:8936–8946.
18. Chen M, Chen Q, Sun X, et al. Generation of retinal ganglion-like cells from reprogrammed mouse fibroblasts. *Invest Ophthalmol Vis Sci*. 2010;51:5970–5978.
19. Vorwerk CK, Lipton SA, Zurakowski D, Hyman BT, Sabel BA, Dreyer EB. Chronic low-dose glutamate is toxic to retinal ganglion cells. Toxicity blocked by memantine. *Invest Ophthalmol Vis Sci*. 1996;37:1618–1624.
20. Johnson TV, Martin KR. Development and characterization of an adult retinal explant organotypic tissue culture system as an in vitro intraocular stem cell transplantation model. *Invest Ophthalmol Vis Sci*. 2008;49:3503–3512.
21. Johnson TV, Bull ND, Martin KR. Identification of barriers to retinal engraftment of transplanted stem cells. *Invest Ophthalmol Vis Sci*. 2010;51:960–970.
22. Vecino E, Ugarte M, Nash MS, Osborne NN. NMDA induces BDNF expression in the albino rat retina in vivo. *NeuroReport*. 1999;10:1103–1106.
23. Teuchner B, Dimmer A, Humpel C, et al. VIP, PACAP-38, BDNF and ADNP in NMDA-induced excitotoxicity in the rat retina. *Acta Ophthalmol*. 2011;89:670–675.
24. Tanaka H, Ito Y, Nakamura S, Shimazawa M, Hara H. Involvement of brain-derived neurotrophic factor in time-dependent neurodegeneration in the murine superior colliculus after intravitreal injection of *N*-methyl-D-aspartate. *Mol Vis*. 2009;15:662–669.
25. Honjo M, Tanihara H, Kido N, Inatani M, Okazaki K, Honda Y. Expression of ciliary neurotrophic factor activated by retinal Müller cells in eyes with NMDA- and kainic acid-induced neuronal death. *Invest Ophthalmol Vis Sci*. 2000;41:552–560.
26. Da Costa R, Roger C, Segelken J, Barben M, Grimm C, Neidhardt J. A novel method combining vitreous aspiration and intravitreal AAV2/8 injection results in retina-wide transduction in adult mice. *Invest Ophthalmol Vis Sci*. 2016;57:5326–5334.
27. Brittis PA, Canning DR, Silver J. Chondroitin sulfate as a regulator of neuronal patterning in the retina. *Science*. 1992;255:733–736.
28. Ohta K, Tannahill D, Yoshida K, Johnson AR, Cook GM, Keynes RJ. Embryonic lens repels retinal ganglion cell axons. *Dev Biol*. 1999;211:124–132.
29. Thompson H, Barker D, Camand O, Erskine L. Slits contribute to the guidance of retinal ganglion cell axons in the mammalian optic tract. *Dev Biol*. 2006;296:476–484.
30. Sanchez-Camacho C, Bovolenta P. Autonomous and non-autonomous Shh signalling mediate the in vivo growth and guidance of mouse retinal ganglion cell axons. *Development*. 2008;135:3531–3541.
31. Deiner MS, Kennedy TE, Fazeli A, Serafini T, Tessier-Lavigne M, Sretavan DW. Netrin-1 and DCC mediate axon guidance locally at the optic disc: loss of function leads to optic nerve hypoplasia. *Neuron*. 1997;19:575–589.
32. Hopker VH, Shewan D, Tessier-Lavigne M, Poo M, Holt C. Growth-cone attraction to Netrin-1 is converted to repulsion by laminin-1. *Nature*. 1999;401:69–73.
33. Ellezam B, Selles-Navarro I, Manitt C, Kennedy TE, McKerracher L. Expression of Netrin-1 and its receptors DCC and

Investigative Ophthalmology & Visual Science

Downloaded from abstracts.iovs.org on 04/20/2024

UNC-5H2 after axotomy and during regeneration of adult rat retinal ganglion cells. *Exp Neurol*. 2001;168:105–115.
34. Petrausch B, Jung M, Leppert CA, Stuermer CA. Lesion-induced regulation of Netrin receptors and modification of Netrin-1 expression in the retina of fish and grafted rats. *Mol Cell Neurosci*. 2000;16:350–364.
35. Teotia P, Van Hook MJ, Fischer D, Ahmad I. Human retinal ganglion cell axon regeneration by recapitulating developmental mechanisms: effects of recruitment of the mTOR pathway. *Development*. 2019;146:dev178012.
36. Kador KE, Alsehli HS, Zindell AN, et al. Retinal ganglion cell polarization using immobilized guidance cues on a tissue-engineered scaffold. *Acta Biomater*. 2014;10:4939–4946.
37. Fligor CM, Langer KB, Sridhar A, et al. Three-dimensional retinal organoids facilitate the investigation of retinal ganglion cell development, organization and neurite outgrowth from human pluripotent stem cells. *Sci Rep*. 2018;8:14520.
38. Honjo M, Tanihara H, Kido N, Inatani M, Okazaki K, Honda Y. Expression of ciliary neurotrophic factor activated by retinal Müller cells in eyes with NMDA- and kainic acid-induced neuronal death. *Invest Ophthalmol Vis Sci*. 2000;41:552–560.
39. Karl MO, Hayes S, Nelson BR, Tan K, Buckingham B, Reh TA. Stimulation of neural regeneration in the mouse retina. *Proc Natl Acad Sci USA*. 2008;105:19508–19513.
40. Takeda A, Shinozaki Y, Kashiwagi K, et al. Microglia mediate non-cell-autonomous cell death of retinal ganglion cells. *Glia*. 2018;66:2366–2384.
41. Tsoka P, Barbisan PR, Kataoka K, et al. NLRP3 inflammasome in NMDA-induced retinal excitotoxicity. *Exp Eye Res*. 2019;181:136–144.
42. Cui Q, Lu Q, So KF, Yip HK. CNTF, not other trophic factors, promotes axonal regeneration of axotomized retinal ganglion cells in adult hamsters. *Invest Ophthalmol Vis Sci*. 1999;40:760–766.
43. Pease ME, Zack DJ, Berlinicke C, et al. Effect of CNTF on retinal ganglion cell survival in experimental glaucoma. *Invest Ophthalmol Vis Sci*. 2009;50:2194–2200.
44. Leaver SG, Cui Q, Plant GW, et al. AAV-mediated expression of CNTF promotes long-term survival and regeneration of adult rat retinal ganglion cells. *Gene Ther*. 2006;13:1328–1341.
45. Gasparini SJ, Llonch S, Borsch O, Ader M. Transplantation of photoreceptors into the degenerative retina: current state and future perspectives. *Prog Retin Eye Res*. 2019;69:1–37.
46. Dick AD. Influence of microglia on retinal progenitor cell turnover and cell replacement. *Eye (Lond)*. 2009;23:1939–1945.
47. Balasubramaniam B, Carter DA, Mayer EJ, Dick AD. Microglia derived IL-6 suppresses neurosphere generation from adult human retinal cell suspensions. *Exp Eye Res*. 2009;89:757–766.
48. Nork TM, Ver Hoeve JN, Poulsen GL, et al. Swelling and loss of photoreceptors in chronic human and experimental glaucomas. *Arch Ophthalmol*. 2000;118:235–245.
49. Charles-Messance H, Blot G, Couturier A, et al. IL-1β induces rod degeneration through the disruption of retinal glutamate homeostasis. *J Neuroinflammation*. 2020;17:1.
50. Wen YT, Ho YC, Lee YC, Ding DC, Liu PK, Tsai RK. The benefits and hazards of intravitreal mesenchymal stem cell (MSC)-based therapies in the experimental ischemic optic neuropathy. *Int J Mol Sci*. 2021;22:2117.

Investigative Ophthalmology & Visual Science

Downloaded from abstracts.iovs.org on 04/20/2024